Short communication

Autogenic reactions for preparing carbon-encapsulated, nanoparticulate TiO_2 electrodes for lithium-ion batteries

Vilas G. Pol [a,*], Sun-Ho Kang [a], Jose M. Calderon-Moreno [b],
Christopher S. Johnson [a], Michael M. Thackeray [a]

[a] *Electrochemical Energy Storage Department, Chemical Sciences and Engineering Division,*
Argonne National Laboratory, 9700 S. Cass Avenue, Argonne, IL 60439, USA
[b] *Institute of Physical Chemistry Ilie Murgulescu, Romanian Academy, 202 Splaiul Independentei St.,*
Bucharest 060021, Romania

ABSTRACT

We report an anhydrous, autogenic technique for synthesizing electronically interconnected, carbon-encapsulated, nanoparticulate anatase anode materials (TiO_2–C) for lithium-ion batteries. The TiO_2–C nanoparticles provide a reversible capacity of $\sim$200 mAh g^{-1}, which exceeds the theoretical capacity of the commercially attractive spinel anode, $Li_4Ti_5O_{12}$ (175 mAh g^{-1}) and is competitive with the capacity reported for other TiO_2 products. The processing method is extremely versatile and has implications for preparing, in a single step, a wide variety of electrochemically active compounds that are coated, *in situ,* with carbon.

© 2010 Elsevier B.V. All rights reserved.

1. Introduction

Significant attention is being paid to the development of lithium-ion batteries for both small- and large-scale devices, such as consumer electronics, power tools, and electrically powered vehicles [1]. Although lithium-ion technology offers the greatest prospect for increasing the energy density of batteries [2], the power capability of these systems is often compromised by the reaction kinetics of the electrode materials. In order to achieve high energy, high power and long life, rapid ionic and electronic transport in stable electrode materials is necessary. Ionic conduction can be enhanced if the electrode materials are synthesized as nanoparticles, when short lithium diffusion distances facilitate access to the full redox capacity of the electrode.

The electronic conductivity of insulating metal oxide- and metal phosphate electrode materials used in lithium-ion cells, can be enhanced either by cation or anion substitution [3] or by electronic wiring of particles, for example, through carbon, conducting polymer, or metal architectures [4,5]. Ideally, the current collecting layer should be thin and uniformly surround each active nanoparticle [6,7]. A well-known example is the cathode material $LiFePO_4$,

for which carbon coatings are used extensively to enhance the electronic conductivity of the electrochemically active nanoparticles in their charged and discharged states [8,9].

In the search for safe materials to replace conventional carbon-based anodes, such as graphite, which reacts with lithium close to the potential of metallic lithium, a considerable effort has been made to exploit TiO_2-based compounds that react with lithium approximately 1.5 V above the lithium potential. The best known and commercially attractive compound is the spinel $Li_4Ti_5O_{12}$ ($2Li_2O \cdot 5TiO_2$), which can accommodate 3 Li$^+$ ions per formula unit without any significant volume change during its transformation to rock-salt $Li_7Ti_5O_{12}$ [10–12]. This reaction is accompanied by the reduction of titanium from a 4+ to an average 3.4+ oxidation state, corresponding to a theoretical electrochemical capacity of 175 mAh g^{-1}. Despite its low capacity, $Li_4Ti_5O_{12}$ ($Li[Ti_{1.67}Li_{0.33}]O_4$) is an extremely high power electrode because (a) the $[Ti_{1.67}Li_{0.33}]O_4$ spinel framework provides an energetically favorable, three-dimensional interstitial space to facilitate fast lithium-ion transport and (b) the parent and lithiated materials are stable as nanoparticles [13]. TiO_2 structures such as anatase [14,15], rutile [16], hollandite [17], and TiO_2-B [18] would be more attractive anodes if, in nanoparticulate form, they could accommodate lithium reversibly and rapidly to the rock-salt stoichiometry $LiTiO_2$ (Ti^{3+}), for which the theoretical capacity is 335 mAh g^{-1}.
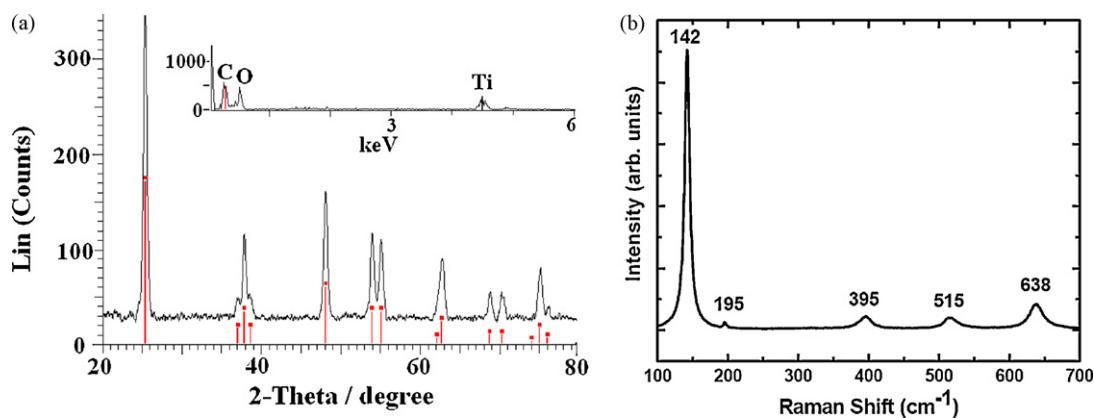
Fig. 1. (a) XRD pattern of anatase TiO_2–C sample, indicating expected peak positions and relative intensities for anatase (inset: EDS spectrum) and (b) Raman spectrum of the same sample.

Although all the above-mentioned TiO_2 compounds have been studied over recent years as possible lithium insertion electrodes for lithium batteries [14–18], limited work has been undertaken to prepare nano-sized, carbon-coated TiO_2–C materials and morphologies to enhance electrochemical properties. Fu et al. [19] prepared TiO_2–C 'core–shell' anode materials via a complex emulsion polymerization of polyacrylonitrile on rutile TiO_2 nanoparticles; these materials provided a capacity of 122 mAh g^{-1} at a 0.25C rate in lithium cells. Lafont et al. [7] described a two-step procedure to coat anatase TiO_2 by first anchoring phenyl phosphonic acid on the surface, followed by thermal treatment under an inert atmosphere.

Herein, we report an anhydrous, solvent-less, autogenic technique for synthesizing electronically interconnected, carbon-encapsulated, nanoparticulate anatase anode materials (TiO_2–C) for lithium-ion batteries. The electrochemical properties of the TiO_2–C product have been evaluated in lithium half cells (against a Li counter electrode) and in lithium-ion full cells (against a high-capacity $0.5Li_2MnO_3 \cdot 0.5LiNi_{0.44}Co_{0.25}Mn_{0.31}O_2$ counter electrode).

2. Experimental

2.1. Synthesis of TiO_2–C

Carbon-encapsulated anatase TiO_2 nanoparticles were prepared by thermolysis of a single precursor, titanium (IV) oxyacetyl acetonate ($TiO[C_5H_8O_2]_2$), in a specially designed (Parr instruments) autogenic reactor (Haynes 230 alloy, 10 mL capacity) fitted with a pressure gauge. Two grams of the precursor material were placed in the reactor under a nitrogen atmosphere. After being tightly sealed, the reactor was placed in a furnace and heated to 700 °C at a heating rate of 30 °C min^{-1}. The temperature of the reactor was held at 700 °C for 1 h, during which a maximum autogenic pressure of 150 psi (10.2 atm) was reached. Thereafter, the reactor was cooled gradually to room temperature, and the remaining pressure released before it was opened to collect the product (a black powder). A thermogravimetric analysis (TGA, Seiko Exstar 6000) revealed that the as-prepared TiO_2 product contained approximately 30% carbon by weight. The product was therefore heated further in air at 450 °C for 1 h to reduce the amount of carbon, leaving a thin layer on the TiO_2 nanoparticles. A subsequent TGA of the heated product showed that approximately 5 wt.% carbon remained in the sample.

2.2. Characterization

Crystallographic information on the TiO_2–C samples was obtained by powder X-ray diffraction with a Siemens D5000 diffrac-

tometer (Cu Kα radiation) at a scan rate of 0.6° 2θ min^{-1}. A Raman spectrum was recorded at room temperature using a triple Jobin Yvon/ Atago-Bussan 92 T-6400 spectrometer, equipped with an Ar 93$^+$ laser ($\lambda = 514.5$ nm) and a liquid-N$_2$ cooled CCD detector. A high-resolution JEOL-7500 field emission scanning electron microscope (FESEM) was employed to study the morphology of the nanocomposite TiO_2–C materials and to obtain a compositional analysis of the samples by energy dispersive X-ray spectroscopy. An aberration (Cs)-corrected high-resolution JEOL-2200 transmission electron microscope equipped with a field emission electron source was employed to undertake elemental mapping across the samples.

2.3. Electrode fabrication

The electrochemical properties of the TiO_2–C materials were evaluated using coin-type cells (2032, Hohsen) assembled in a helium-filled glove box. The electrodes consisted of 85 wt% TiO_2–C, 8 wt% acetylene black, and 7 wt% polyvinylidene difluoride (PVDF) binder on a carbon-coated aluminum foil; the average active-material loading density was 3.8 mg cm^{-2}. The counter electrodes were either metallic lithium (half cell) or $0.5Li_2MnO_3 \cdot 0.5LiNi_{0.44}Co_{0.25}Mn_{0.31}O_2$ (full cell). The latter electrode consisted of 80 wt% $0.5Li_2MnO_3 \cdot 0.5LiNi_{0.44}Co_{0.25}Mn_{0.31}O_2$, 5 wt% acetylene black, 5 wt% graphite, and 10 wt% PVDF binder on aluminum foil with an average active-material loading density of 3.5 mg cm^{-2}, such that the TiO_2–C/$0.5Li_2MnO_3 \cdot 0.5LiNi_{0.44}Co_{0.25}Mn_{0.31}O_2$ lithium-ion cells were constructed to be anode limited. The uniformly coated carbon network on the TiO_2 nanoparticles facilitated the fabrication of a homogeneous, smooth laminate compared to those prepared from bare TiO_2 nanoparticles. The electrolyte was 1.2 M LiPF$_6$ in a 3:7 (by volume) mixture of ethylene carbonate and ethyl methyl carbonate. The Li/TiO_2–C half cells were cycled galvanostatically between 1.1 and 2.35 V at a rate of 16.3 mA g^{-1} ($\sim$C/17), whereas the TiO_2–C/$0.5Li_2MnO_3 \cdot 0.5LiNi_{0.44}Co_{0.25}Mn_{0.31}O_2$ lithium-ion cells were cycled between 0.05 and 3.5 V at 18 mA g^{-1} ($\sim$C/12). Rate studies of the Li/TiO_2–C half cells were carried out using current densities that ranged from 16.3 ($\sim$C/17) to 196 mA g^{-1} ($\sim$C/1). The reported charge/discharge capacities are based solely on the active mass of TiO_2 used in the electrodes.

3. Results and discussion

The X-ray diffraction (XRD) pattern of a TiO_2–C product prepared by the autogenic reaction of $TiO[C_5H_8O_2]_2$ at 700 °C and 150 psi (10.2 atm), followed by combustion in air to reduce the car-

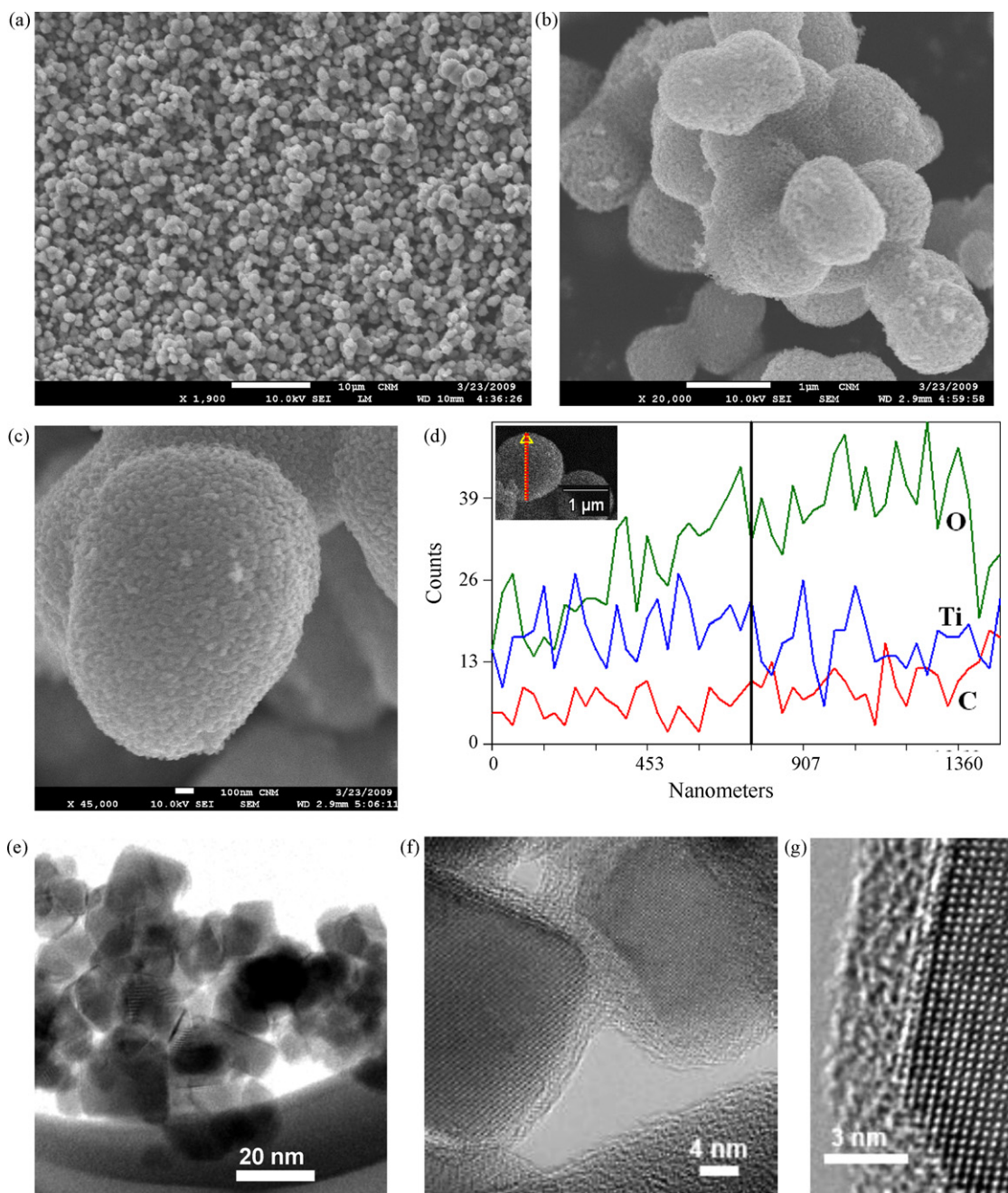**Fig. 2.** (a–c) Field emission scanning electron microscope images of TiO$_2$–C at different magnifications, (d) line-scan mapping of a secondary TiO$_2$–C particle, and (e–g) high-resolution TEM of TiO$_2$–C at different magnifications.

bon content to 5%, is provided in Fig. 1a. The diffraction peaks match those of tetragonal anatase TiO$_2$ (space group symmetry I4$_1$/amd). An elemental analysis of the TiO$_2$–C sample by energy dispersive X-ray spectroscopy (EDS) showed only C, O, and Ti, confirming the purity of TiO$_2$ and the presence of carbon (inset in Fig. 1a). A Raman spectrum of the TiO$_2$–C product, with the strongest band at 142 cm^{-1} and additional bands at 195, 395, 515, and 638 cm^{-1}, is characteristic of pure anatase TiO$_2$ [11] (Fig. 1b). Two weak Raman bands (not shown in Fig. 1b) provided some information about the structural character of the encapsulating, X-ray amorphous carbon layer: one at 1343 cm^{-1} (D-band), corresponds to dangling bonds in in-plane terminated disordered graphite, and the other at 1595 cm^{-1} (G-band), corresponds to the *E2g* mode related to the vibration of sp^2-bonded carbon atoms in a two-dimensional hexagonal graphene layer [20]. Kostecki and co-workers have also

employed Raman spectroscopy to characterize analogous carbon coatings on LiFePO$_4$ electrode materials [21,22]. From their studies, they concluded: (1) the relative peak heights and widths of the D- and G bands change substantially with the pyrolysis temperature and the nature of the precursor materials, (2) the variation of the width and intensity of the D- and G bands is related to the growth and size of different carbon phases, and the presence of functional groups and impurities, and (3) a more graphitic carbon coating results in higher electronic conductivity of the composite LiFePO$_4$/C electrode, thereby improving the electrochemical performance of the cells.

Scanning electron microscopy (SEM) images of the TiO$_2$–C particles are shown, with increasing magnification, in Fig. 2a–c; they depict oval- and spherical-shaped secondary particles, 0.5–3 μm in dimension, often connected together (Fig. 2b), enhancing the
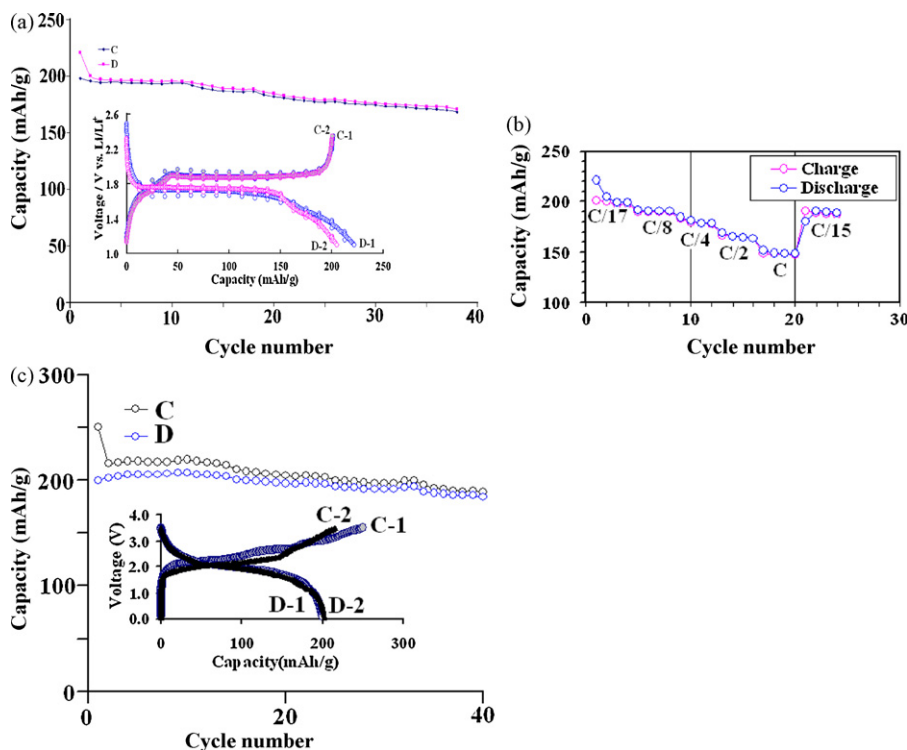
Fig. 3. (a) Cycling behavior of Li/TiO$_2$–C half cells (1.1–2.5 V, 16.3 mA g^{-1}, C/17 rate), (b) rate performance of Li/TiO$_2$–C cells, and (c) cycling behavior of a TiO$_2$–C/0.5Li$_2$MnO$_3$·0.5LiNi$_{0.44}$Co$_{0.25}$Mn$_{0.31}$O$_2$ lithium-ion cell (0.05–3.5 V, 18 mA g^{-1}, C/12 rate).

integrity of the TiO$_2$–C matrix. Fig. 2c shows that individual secondary TiO$_2$ particles consist of significantly smaller (<30 nm) particles. Elemental line-scan mapping across a micron-sized, spherical secondary TiO$_2$ particle (Fig. 2d) verified the presence of a minor amount of C and higher amounts of Ti and O; it also confirmed that the particles did not contain impurities, as did several independent elemental dot mapping evaluations of other TiO$_2$–C particles.

The high-resolution TEM image (Fig. 2e) shows that most of the primary TiO$_2$–C particles are, on average, less than ~20 nm in dimension, and that they are highly crystalline, consistent with the XRD data. Fig. 2f and g are, in general, representative images of the whole TiO$_2$–C sample; *they demonstrate the likelihood that most, if not all, the TiO$_2$ nanoparticles are encapsulated by a layer of amorphous carbon*, in this case typically 2–4 nm, the thickness of which can be tailored by the temperature and length of the carbon combustion process (as described in Section 2). Previously, it has been reported that the phase transformation [23] of pure anatase to rutile occurs at around 600 °C. Our XRD data, however, demonstrate that the anatase phase, when coated with carbon by the autogenic process, can be sustained above this transformation temperature even when the reaction is conducted at 800 °C in an inert atmosphere. The suppression of the phase transition has been tentatively attributed, in a related study, to the presence of a carbon shell around the TiO$_2$ nanoparticles [24], consistent with the results and interpretation given by Inagaki et al. [25], in their independent study of carbon-coated TiO$_2$.

The electrochemical properties of nanocomposite TiO$_2$–C electrodes are shown in Fig. 3(a–c). Fig. 3a shows the initial two discharge/charge curves of a Li/TiO$_2$–C half cell, cycled at a constant current density of 16.3 mA g^{-1} (~C/17 rate) between 1.1 and 2.35 V, as well as the corresponding capacity vs. cycle number plot. Discharge of the Li/TiO$_2$–C cell takes place in two discrete steps. The first step occurs on a voltage plateau at approximately 1.73 V, which is consistent with the intercalation of lithium into the anatase

structure [14,15]; this plateau corresponds to an electrochemical capacity of approximately 150 mAh g^{-1} or, alternatively, the uptake of ~0.45 Li per TiO$_2$ unit. The second step is a steadily sloping voltage region between 1.5 and 1.1 V, delivering a further capacity of 50–60 mAh g^{-1}. It is noteworthy that our interconnected TiO$_2$–C particles show higher initial cycle efficiency (~89.5%) compared to previous reports (~70% [14] and ~80% [7]). The autogenically prepared TiO$_2$ electrode provides a better rechargeable capacity (~200 mAh g^{-1} at a C/17 rate) compared to the nanoparticulate anatase TiO$_2$ products (without the carbon coating) prepared by hydrolysis of titanium isopropoxide followed by a 1-h anneal at 250 °C (~150 mAh g^{-1} at a C/20 rate) [14]. Furthermore, the capacity delivered by the autogenically prepared TiO$_2$–C electrodes exceeds the theoretical value of the lithium titanate spinel, Li$_4$Ti$_5$O$_{12}$ (175 mAh g^{-1}) [10,26], which is currently being exploited as an anode in lithium-ion battery products by Altairnano, Enerdel Inc., and Toshiba Corp., amongst others. The reversibility of the 1.5–1.1 V region of the electrochemical profile (Fig. 3a), even at higher rates (Fig. 3b), indicates that a redox reaction of lithium with the anatase TiO$_2$ component occurs, consistent with the maximum uptake at $x \approx 0.7$ in Li$_x$TiO$_2$ as reported by Murphy et al. [27], with possible faradaic contributions from the amorphous carbon layers that surround the TiO$_2$ particles. Note that our autogenically prepared TiO$_2$–C electrodes deliver 150 mAh g^{-1} at a reasonably fast (C/1) rate, corresponding to the typical maximum uptake of Li by the anatase TiO$_2$ structure under slower reaction conditions [14,15], and that higher capacity can be regained by reverting to lower current rates (e.g., C/15, Fig. 3b).

The initial two discharge/charge curves of an anode limited lithium-ion cell, TiO$_2$–C/0.5Li$_2$MnO$_3$·0.5LiNi$_{0.44}$Co$_{0.25}$Mn$_{0.31}$O$_2$, cycled between 0.05 and 3.5 V at a constant current density of 18 mA g^{-1} (~C/12 rate), as well as the corresponding capacity vs. cycle number plot, are provided in Fig. 3c. The lithium- and manganese-rich layered 0.5Li$_2$MnO$_3$·0.5LiNi$_{0.44}$Co$_{0.25}$Mn$_{0.31}$O$_2$ cathode, alternatively Li$_{1.2}$Mn$_{0.525}$Ni$_{0.175}$Co$_{0.100}$O$_2$ in standard

layered notation, is a member of the family of structurally integrated, high-capacity $x\text{Li}_2\text{MnO}_3\cdot(1-x)\text{LiMO}_2$ (M = Mn, Ni, Co) compounds [28]. When charged above 4.6 V vs. Li^0, a process that activates the Li_2MnO_3 component by Li_2O extraction and leaves an electrochemically active MnO_2 component within the structure, very high capacities (>200 mAh g^{-1}) can be delivered by the $0.5\text{Li}_2\text{MnO}_3\cdot0.5\text{LiNi}_{0.44}\text{Co}_{0.25}\text{Mn}_{0.31}\text{O}_2$ electrode at moderate rates [29]. The electrochemical profiles in Fig. 3c demonstrate that the lithium ions, extracted from the $\text{LiNi}_{0.44}\text{Co}_{0.25}\text{Mn}_{0.31}\text{O}_2$ and Li_2MnO_3 components of the cathode in this cell configuration above ~2 and ~2.6 V, respectively, are intercalated into the TiO_2–C anode during the initial charge; the irreversible capacity loss on the first cycle is 20%. The cycling data indicate that, in this cell configuration, approximately 200 mAh g^{-1} can be delivered by both the anode and cathode. The data auger well for future improvements and the development of safe TiO_2–C/$x\text{Li}_2\text{MnO}_3\cdot(1-x)\text{LiMO}_2$ cells that should provide higher energy than lithium-ion cells with $\text{Li}_4\text{Ti}_5\text{O}_{12}$ spinel anodes.

4. Conclusions

The autogenic process described in this paper, which amounts essentially to an anhydrous autoclave reaction, has implications for designing and preparing a wide range of nanoparticulate anode and cathode materials for both lithium-ion battery and supercapacitor applications. Of particular interest are nano-sized lithium-battery electrode materials of commercial significance, such as $\text{Li}_4\text{Ti}_5\text{O}_{12}$, the family of olivine LiMPO_4 (M = Fe, Mn, Ni, Co) compounds, metals (e.g., Sn), intermetallic compounds (e.g., CoSn), and Si, as well as carbon spheres and nanotubes. Work on these materials is in progress, the results of which will be presented in forthcoming papers.

Acknowledgements

References

[1] Y.G. Guo, Y.-S. Hu, W. Sigle, J. Maier, Adv. Mater. 19 (2007) 2087–2091.
[2] K. Kang, Y.S. Meng, J. Breger, C.P. Grey, G. Ceder, Science 311 (2006) 977–980.
[3] S.B. Schougaard, J. Breger, M. Jiang, C.P. Grey, J.B. Goodenough, Adv. Mater. 18 (2006) 905–909.
[4] P.S. Herle, B. Ellis, N. Coombs, L.F. Nazar, Nat. Mater. 3 (2004) 147–152.
[5] P.L. Taberna, S. Mitra, P. Poizot, P. Simon, J.M. Tarascon, Nat. Mater. 5 (2006) 567–573.
[6] R. Dominko, M. Gaberscek, J. Drofenik, M. Bele, J. Jammik, Electrochem. Acta 48 (2003) 3709–3716.
[7] U. Lafont, L. Simonin, M. Gaberscek, E.M. Kelder, J. Power Sources 174 (2007) 1104–1108.
[8] Y. Wang, Y. Wang, E. Hosono, K. Wang, H. Zhou, Angew. Chem. Int. Ed. 47 (2008) 7461–7465.
[9] K.S. Park, S.B. Schougaard, J.B. Goodenough, Adv. Mater. 19 (2007) 848–851.
[10] K.M. Colbow, J.R. Dahn, R.R. Hearing, J. Power Sources 26 (1989) 397–402.
[11] E. Ferg, R.J. Gummow, A. De Kock, M.M. Thackeray, J. Electrochem. Soc. 141 (1994) L147–L150.
[12] A.N. Jansen, A.J. Kahaian, K.D. Kepler, P.A. Nelson, K. Amine, D.W. Dees, D.R. Vissers, M.M. Thackeray, J. Power Sources 81 (1999) 902–905.
[13] A. Singhal, G. Skandan, G. Amatucci, F. Badway, N. Ye, A. Manthiram, H. Ye, J.J. Xu, J. Power Sources 129 (2004) 38–44.
[14] G. Sudant, E. Baudrin, D. Larcher, J.-M. Tarascon, J. Mater. Chem. 15 (2005) 1263–1269.
[15] A. Stashans, S. Lunell, R. Bergstrom, A. Hagfeldt, S.E. Lindquist, Phys. Rev. B 53 (1996) 159–170.
[16] E. Baudrin, S. Cassaignon, M. Koesch, J.P. Jolivet, L. Du Pont, J.M. Tarascon, Electrochem. Commun. 9 (2007) 337–342.
[17] L.D. Noialles, C.S. Johnson, J.T. Vaughey, M.M. Thackeray, J. Power Sources 81 (1999) 259–263.
[18] A.R. Armstrong, G. Armstrong, J. Canales, R. Garcia, P.G. Bruce, Adv. Mater. 17 (2005) 862–865.
[19] L.J. Fu, H. Liu, H.P. Zhang, C. Li, T. Zhang, J.P. Wu, R. Holze, H.Q. Wu, Electrochem. Commun. 8 (2006) 1–4.
[20] A. Odani, V.G. Pol, S.V. Pol, M. Koltypin, A. Gedanken, D. Aurbach, Adv. Mater. 18 (2006) 1431–1436.
[21] M.M. Doeff, Y. Hu, F. McLarnon, R. Kostecki, Electrochem. Solid State Lett. 6 (2003) A207–A209.
[22] J.D. Wilcox, M.M. Doeff, M. Marcinek, R. Kostecki, J. Electrochem. Soc. 154 (2007) A389–A395.
[23] V.G. Pol, A. Zaban, Langmuir 23 (2007) 11211–11216.
[24] S.V. Pol, V.G. Pol, A. Gedanken, Chem. Eur. J. 10 (2004) 4467–4473.
[25] M. Inagaki, Y. Hirose, T. Matsunaga, T. Tsumura, M. Toyoda, Carbon 41 (2003) 2619–2624.
[26] C.H. Chen, J.T. Vaughey, A.N. Jansen, D.W. Dees, A.J. Kahaian, T. Goacher, M.M. Thackeray, J. Electrochem. Soc. 148 (2001) A102–A104.
[27] D.W. Murphy, R.J. Cava, S.X. Zahurak, A. Santoro, Solid State Ionics 9–10 (1983) 147–413.
[28] M.M. Thackeray, S.-H. Kang, C.S. Johnson, J.T. Vaughey, R. Benedek, S.A. Hackney, J. Mater. Chem. 17 (2007) 3112–3125.
[29] S.-H. Kang, C.S. Johnson, J.T. Vaughey, K. Amine, M.M. Thackeray, J. Electrochem. Soc. 153 (2006) A1186–A1192.